View metadata, citation and similar papers at core.ac.uk
brought to you by CORE
provided by EPub Bayreuth

The Plant Journal

The Plant Journal (2020) **103,** 995–1009 doi: 10.1111/tpj.14779

A mutation in the essential and widely conserved DAMAGED DNA BINDING1-Cullin4 ASSOCIATED FACTOR gene *OZS3* causes hypersensitivity to zinc excess, cold and UV stress in *Arabidopsis thaliana*

Michael Weber[†], Blen Beyene[†], Nicole Nagler[†], Jörn Herfert, Stefanie Schempp, Maria Klecker and Stephan Clemens[*]
Department of Plant Physiology, University of Bayreuth, Bayreuth 95440, Germany

Received 2 May 2018; revised 18 February 2020; accepted 1 April 2020; published online 20 April 2020.
*For correspondence (e-mail stephan.clemens@uni-bayreuth.de).
[†]These authors contributed equally to this work.

SUMMARY

The *overly zinc sensitive Arabidopsis thaliana* mutant *ozs3* shows reduced growth of the primary root, which is exacerbated by an excess specifically of Zn ions. In addition, *ozs3* plants display various subtle developmental phenotypes, such as longer petioles and early flowering. Also, *ozs3* seedlings are completely but reversibly growth-arrested when shifted to 4°C. The causal mutation was mapped to a gene encoding a putative substrate-recognition receptor of cullin4 E3 ligases. *OZS3* orthologous genes can be found in almost all eukaryotic genomes. Most species from *Schizosaccharomyces pombe* to *Homo sapiens*, and including *A. thaliana*, possess one ortholog. No functional data are available for these genes in any of the multicellular model systems. CRISPR-Cas9-mediated knockout demonstrated that a complete loss of *OZS3* function is embryo-lethal, indicating essentiality of *OZS3* and its orthologs. The OZS3 protein interacts with the adaptor protein DAMAGED DNA BINDING1 (DDB1) in the nucleus. Thus, it is indeed a member of the large yet poorly characterized family of DDB1-cullin4 associated factors in plants. Mutant phenotypes of *ozs3* plants are apparently caused by the weakened DDB1–OZS3 interaction as a result of the exchange of a conserved amino acid near the conserved WDxR motif.

Keywords: ***Arabidopsis thaliana*, cold sensitivity, E3 ligases, metal tolerance, WDR70.**

INTRODUCTION

Throughout their life cycle, plants have to cope with various abiotic stress factors. These include not only drought, cold, heat, or hypoxia, but also inhibitory concentrations of minerals in the soil. Besides the more common threats salt and aluminum, plant roots can be exposed to metal pollutants such as cadmium (Cd) and arsenic (As), or to an excess of essential microelements (Clemens, 2006; Nagajyoti *et al.*, 2010; Kopittke *et al.*, 2010). Among the latter is zinc (Zn). Potentially toxic Zn concentrations in soil are mostly a result of human activities such as the application of Zn-rich animal manure or sewage sludge to agricultural fields. Although Zn deficiency is clearly a more common problem for plant productivity, Zn excess does occur (Alloway, 2008; Zhao *et al.*, 2015a,b).

Among the microelements, Zn has been recruited for a particularly wide range of biological functions. Almost 10% of all eukaryotic proteins are estimated to bind Zn(II) (Andreini *et al.*, 2006). The available knowledge mainly for mammalian systems suggests that Zn(II) has not only structural and catalytic roles, but also various regulatory functions; for example, the modulation of enzyme activities and signaling pathways (Kambe *et al.*, 2015). One example is the key role of a Zn transporter in controlling the pulmonary vascular responses to chronic hypoxia (Zhao *et al.*, 2015a,b). It appears highly likely that Zn(II) influences many cellular pathways in plants as well, given the similar number of predicted Zn(II) binding sites in mammalian and plant proteins. However, whether and to what extent this is the case currently remains unknown.

A key aspect of Zn biology is the control over labile cytosolic Zn, such that Zn(II) is not tightly bound by proteins and available for ligand exchange (Sinclair and Krämer, 2012; Zlobin *et al.*, 2019). In *Arabidopsis thaliana* root cells, the estimated concentration of this pool is around 400 pM, whereas total cellular Zn amounts to

© 2020 The Authors.
The Plant Journal published by Society for Experimental Biology and John Wiley & Sons Ltd
This is an open access article under the terms of the Creative Commons Attribution License,
which permits use, distribution and reproduction in any medium, provided the original work is properly cited.

around 50 μM (Lanquar *et al.*, 2014). Zn toxicity occurs when labile cytosolic Zn(II) exceeds 2 μM. Zn(II) then interacts with nitrogen, oxygen or sulfur ligands in an uncontrolled way (Krężel and Maret, 2016). The ability of a plant cell to tolerate Zn excess is largely dependent on the capacity to suppress such potentially detrimental interactions. Consequently, mutants lacking vacuolar Zn transporters such as MTP1 and MTP3 (Arrivault *et al.*, 2006; Kawachi *et al.*, 2009), Zn ligand transporters (e.g. ZIF1) (Haydon and Cobbett, 2007) or Zn ligands (e.g. phytochelatins) (Kühnlenz *et al.*, 2016) are Zn hypersensitive. At the same time, these proteins and ligands are key factors of Zn homeostasis because they are involved in partitioning Zn between plant tissues and organs. Moreover, the biological functions of Zn(II) depend on the controlled modulation of cytosolic Zn(II) (Maret, 2017), as in the above-mentioned mammalian example. Therefore, a possible approach for identifying Zn-affected pathways and to make inroads into mechanistically understanding Zn biology is to screen for mutants with compromised Zn tolerance. This is exemplified by the recent identification of a pathway controlling photomorphogenesis, via the characterization of a Zn hypersensitive mutant (Sinclair *et al.*, 2017). Another Zn tolerance screen resulted in the identification of several *overly Zn sensitive* (*ozs*) *A. thaliana* mutants (Weber *et al.*, 2013). In the present study, we report on *ozs3*. The phenotypes of this mutant are caused by a mutation in a gene encoding a DWD (DDB1 binding WD40) protein.

The regulation of many plant responses to abiotic stress factors (similar to the regulation of myriad developmental and physiological processes in eukaryotes in general) is dependent on E3 ligases (Deshaies and Joazeiro, 2009; Guo *et al.*, 2013). These enzymes confer specificity to the proteasomal degradation of proteins by mediating the transfer of ubiquitin moieties onto target proteins. More than 1500 different E3 ligases are encoded in the *A. thaliana* genome (Hua and Vierstra, 2011), indicating the complexity of the machinery for controlled removal of proteins from cells. Cullin-RING ubiquitin ligases (CRLs) represent the largest class of E3 ligases, comprising E3 complexes with more than 800 different adaptor proteins in *A. thaliana* (Hua and Vierstra, 2011). CRLs consist of cullin proteins as scaffold, associated C-terminally with the RING-finger protein RBX1 and N-terminally with proteins involved in substrate recruitment. In plants, three main cullin types have been found: CUL1/CUL2, CUL3a/b and CUL4 (Hua and Vierstra, 2011). They differ in terms of the substrate-recruiting modules that they interact with. Typical for the more recently identified CUL4 is interaction with DWD proteins (Biedermann and Hellmann, 2011). DWD proteins, alternatively referred to as DCAFs (for DDB1-CUL4 ASSOCIATED FACTOR) (Angers *et al.*, 2006), do not directly bind to CUL4. Instead, DDB1 (DAMAGED DNA BINDING1) proteins serve as adaptors linking CUL4 with DWD proteins as the actual substrate-recognition receptors (Lee and Zhou, 2007). In *A. thaliana*, two different DDB1 proteins exist, DDB1a and b (Schroeder *et al.*, 2002; Bernhardt *et al.*, 2010), which are assumed to interact with 85 different DWD proteins. In rice, the number of putative DWD proteins is 78 (Lee *et al.*, 2008). A defining characteristic of DWDs is the so-called DWD box, a conserved 16–17 amino acid stretch that ends in an aspartate-arginine motif (WDxR) (Biedermann and Hellmann, 2011). The WDxR motif is critical for interaction with DDB1 (Angers *et al.*, 2006; He *et al.*, 2006).

Few DWD proteins in plants have been functionally characterized to date (Shu and Yang, 2017). The *A. thaliana* homolog of human DCAF1 forms a nuclear complex with CUL4 and DDB1. T-DNA insertion mutants showed arrest of embryonic development, whereas *DCAF1* co-suppression caused multiple developmental phenotypes (Zhang *et al.*, 2008). The DWD protein WDR55 is required for gametogenesis and seed development (Bjerkan *et al.*, 2012). Most other studied DWD proteins have been implicated in responses to abiotic factors (Seo *et al.*, 2014; Ren *et al.*, 2019). A DWD protein found to be involved in metal toxicity responses is TANMEI/ALT2 (Nezames *et al.*, 2012). Loss-of-function mutants were isolated in a screen for suppressors of aluminum hypersensitivity. TANMEI/ALT2 is involved in DNA damage control and mediates active growth arrest when *A. thaliana* roots are exposed to aluminum.

In the present study, we report on the characterization of the *ozs3* mutant and the identification of the causal mutation. Our data show that *OZS3* encodes an essential DWD protein interacting with DDB1, presumably as part of a CUL4 E3 ligase complex. The mutation in *ozs3* does not completely abolish function, although it weakens the interaction with DDB1.

RESULTS

ozs3 phenotypes

The *ozs3* line belongs to group 2 of the isolated Zn^{2+} hypersensitive mutants (Weber *et al.*, 2013), such that, unlike the previously characterized *ozs1* and *ozs2* mutants, it showed reduced root growth already under control conditions. An excess of Zn^{2+} was the only tested metal excess condition that caused a stronger reduction in relative root growth compared to the wild-type Col-0 (Weber *et al.*, 2013). Relative root growth of *ozs3* compared to Col-0 was unaffected by approximately half-maximally inhibiting concentrations of Cd^{2+}, Cu^{2+}, Fe^{2+}, Mn^{2+}, Co^{2+} or Ni^{2+} (Figure S1a). We studied the specific impact of Zn^{2+} excess in more detail with two independent backcross (BC) lines. Zn^{2+} hypersensitivity relative to Col-0 was apparent already in the presence of 20 μM Zn^{2+} (Figure S2). For seedlings assayed after 7 days, the difference between wild-type and

© 2020 The Authors.

ozs3 under control conditions was less pronounced than after 12 days, the time when the *ozs* mutants were initially scored (Weber *et al.*, 2013). Zn^{2+} hypersensitivity was again highly significant (Figure 1a,b). When growth was monitored continuously over 9 days, it became apparent that, on control medium, *ozs3* seedlings grow like Col-0 up to approximately day 5. From day 6 onward, the difference in primary root length was significant (Figure 1c,d) because, after day 4, the growth rate of Col-0 increased, whereas that of *ozs3* decreased. In the presence of elevated Zn^{2+} (60 μM), root growth of *ozs3* seedlings was more strongly reduced than that of Col-0 seedlings already 2 days earlier. Furthermore, the difference in primary root growth between Col-0 and *ozs3* after 4 days was exacerbated by Zn^{2+} excess.

A typical secondary stress caused by metal exposure is an increase in the concentrations of reactive oxygen species (ROS). We determined ROS levels in wild-type and mutant seedlings after growth under control conditions and in the presence of growth-inhibitory Zn^{2+} concentrations. Although wild-type seedlings showed only a minor increase in H_2O_2 levels when exposed to Zn excess, H_2O_2 levels in the two *ozs3* backcross lines rose to a concentration that was approximately twice as high compared to wild-type (Figure 2a). This difference was even higher when considering the lower background level in *ozs3* seedlings under control conditions. O_2^- staining qualitatively confirmed higher ROS levels in Zn-exposed *ozs3* seedlings (Figure 2b). These data indicated a deficiency of *ozs3* mutant seedlings in limiting oxidative stress elicited by Zn excess. Elemental analysis of seedlings showed that this higher level of stress was not the result of a stronger Zn accumulation. There were no significant differences between Col-0 and mutant in Zn contents of roots and shoots, neither under control conditions, nor after Zn^{2+} exposure (Figure S3).

Next, we tested the effects of other abiotic stress factors. Salt stress influenced the relative root growth of wild-type

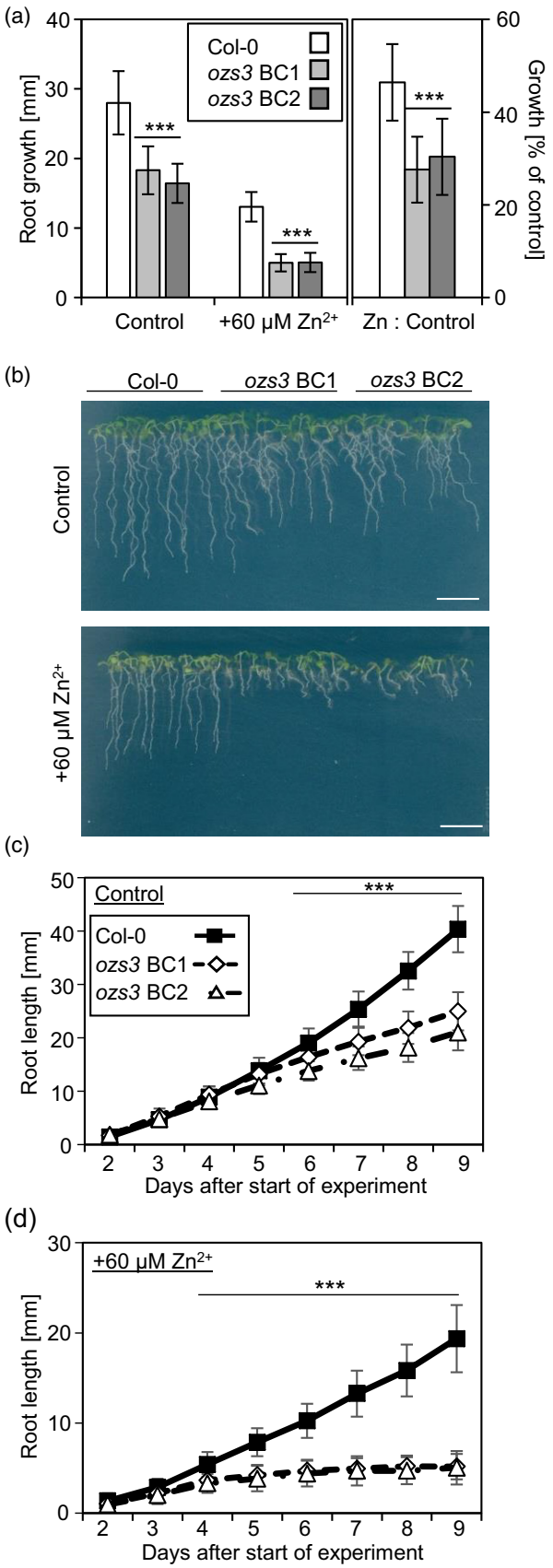

Figure 1. The *ozs3* mutant is Zn^{2+} hypersensitive and shows a root growth defect.
(a, b) Seedlings of Col-0 (white bars) and two independent *ozs3* backcross lines (BC) (grey bars) were grown vertically under control conditions or in the presence of additional 60 μM $ZnSO_4$ for approximately 7 days. Data in (a) represent the mean ± SD of three independent experiments (n = 52–53). Left: absolute root growth. Significant differences from wild-type were determined by two-way analysis of variance (ANOVA) and Tukey's test (***$P < 0.001$). Right: relative root growth of seedlings as an indicator for tolerance, calculated as root length metal treatment/mean root length control conditions × 100. Significant differences from Col-0 were determined by one-way ANOVA and Tukey's test (***$P < 0.001$). Shown in (b) are seedlings after 7 days cultivation. Scale bar = 1 cm.
(c, d) Length of primary roots of Col-0 (filled symbols) and the two independent *ozs3* backcross lines (BC) (open symbols), grown vertically under control (c) and Zn^{2+} excess conditions (= 60 μM) (d), was monitored for 9 days. Data represent the mean ± SD of three independent experiments (n = 21–24). Statistical analysis was performed for every time point by a t-test. Asterisks indicate significant differences of both BC lines to Col-0 (***$P < 0.001$).

© 2020 The Authors.

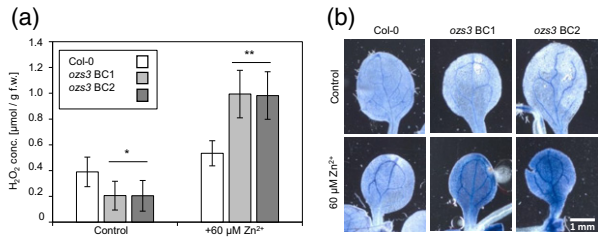

Figure 2. Zn^{2+} excess conditions cause enhanced reactive oxygen species (ROS) accumulation in *ozs3* seedlings. Seedlings of Col-0 (white bars) and two independent *ozs3* backcross lines (BC) (grey bars) were grown vertically under control conditions or in the presence of additional 60 µM $ZnSO_4$ for 12 days.
(a) H_2O_2 accumulation was quantified using 3,3′-diaminobenzidine staining. Data represent the mean ± SD of three independent experiments ($n = 6$). Statistical analysis was performed by a *t*-test. Asterisks indicate significant differences to Col-0 (*$P < 0.05$; **$P < 0.01$).
(b) O_2^- accumulation was visualized by nitroblue tetrazolium chloride staining. The images show representative leaves.

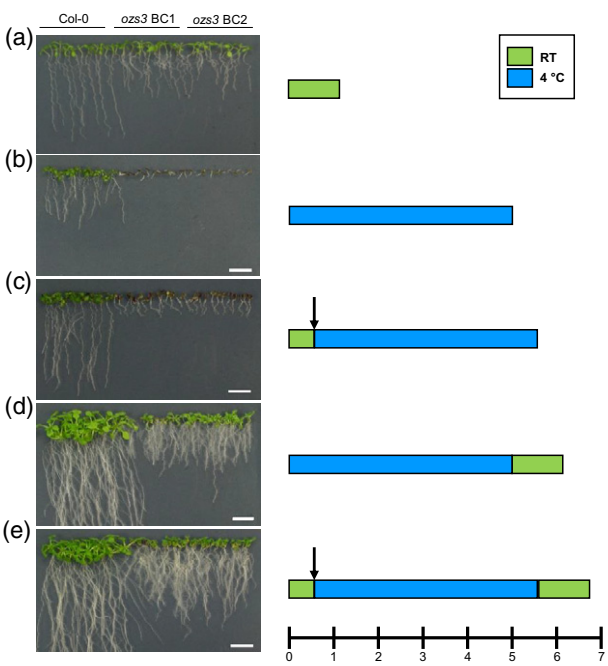

Figure 3. *ozs3* shows growth arrest at low temperatures.
Seedlings of Col-0 and two *ozs3* backcross lines (BC) were grown vertically for 8 days at room temperature (RT) (green bars) (a), for 5 weeks at 4°C (blue bars) (b), or for 4 days at RT followed by 5 weeks at 4°C (c). Arrows indicate the shift to cold. Survival of seedlings was tested by transferring seedlings shown in (b) and (c) to RT for 8 days (d and e, respectively). Scale bar = 1 cm.

and *ozs3* mutant seedlings to a similar extent, whereas osmotic and oxidative stress affected relative root growth of *ozs3* seedlings less than that of Col-0 seedlings (Figure S1b). By contrast, cold treatment had a dramatic inhibitory effect on *ozs3*. Seedlings managed to germinate, although they were unable to grow at 4°C (Figure 3a,b). Transfer of seedlings to cold conditions after 4 days at room temperature caused an immediate growth arrest (Figure 3c). However, seedlings stayed alive under these conditions. Following transfer back to room temperature, *ozs3* seedlings resumed growth and, within 8 days, they developed the typical control condition phenotype, comprising shorter primary roots compared to Col-0 (Figure 3d,e).

When *ozs3* backcross lines were cultivated side-by-side with Col-0 under various non-stress conditions, several morphological and developmental phenotypes became apparent. An altered root morphology of the *ozs3* mutant was observed when seedlings were grown on agar plates for 12 days (Figure S4). Compared to Col-0, specifically growth of the primary root was inhibited in *ozs3*, whereas the lateral roots grew normally (Figure S4b). This resulted in a higher lateral root index and a higher lateral root density for the BC lines (Figure S4c,d). Flowering occurred earlier in *ozs3* mutants, as was apparent from the smaller number of rosette leaves at the time of flowering (Figure S5). After 8 weeks on the soil under short-day conditions, the petiole length of *ozs3* plants was increased by approximately 15–20% relative to Col-0 (Figure S6b).

Identification of the causal gene

Wild-type growth of F1 plants and the segregation of the root growth phenotype in F2 backcross populations were indicative of a recessive nature of the *ozs3* mutation. The *ozs3* mutation was localized to the lower arm of chromosome 2. The sequencing of 14 open reading frames within the mapped interval revealed a single mutation in the gene *At2g20330*. The C to T mutation in the coding sequence of the *At2g20330* gene changes amino acid 377 from threonine to isoleucine in the corresponding protein (Figure 4a). An alignment of orthologous sequences from a wide phylogenetic range showed that amino acid 377 in OZS3 is highly conserved (Figure 4b). To verify that the mutation in *At2g20330* was causal for the *ozs3* phenotypes, one of the *ozs3* backcross lines was transformed with a DNA fragment including 1.5 kb of the promoter, the coding sequence plus the 5′ and 3′-UTRs, and 450 bp of the terminator of *At2g20330*. The root growth phenotype under control conditions as well as the Zn^{2+} hypersensitivity was fully complemented in the transformed lines (Figure 4c,d). The same was found for the chilling sensitivity, the increase in petiole length and the early flowering phenotype of mature *ozs3* plants (Figure S6). We therefore named the gene *At2g20330 OZS3*.

OZS3 transcript abundance was comparable in roots and shoots. No up- or downregulation upon exposure to Zn excess was detectable (Figure S7a). This is consistent with a lack of responsiveness to abiotic or biotic stresses apparent from data deposited in Genevestigator (https://genevestigator.com). To analyze *OZS3* expression patterns,

© 2020 The Authors.

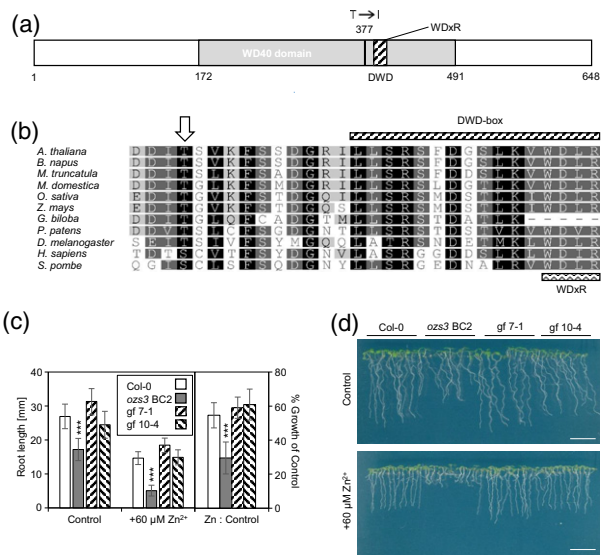

Figure 4. The causal mutation in *ozs3* affects a highly conserved amino acid in the DWD protein At2g20330.

(a) Domain structure of OZS3. Numbers indicate positions of amino acids. Bold black line marks the amino acid change caused by the mutation in *ozs3* (Thr to Ile at position 377); grey: WD40 domain; the DWD (= DDB1 binding WD40 domain) containing the WDxR motif is highlighted as a striped box.

(b) Most eukaryotes possess one *OZS3* ortholog. Partial amino acid sequence alignment of the WD40 domain for OZS3 and orthologs from higher plants, mosses, animals and yeast: *Arabidopsis thaliana* (NP_179623.1), *Brassica napus* (XP_013652708.1), *Medicago truncatula* (XP_003625415.1), *Malus domestica* (XP_008349006.2), *Oryza sativa* (XP_015614481.1), *Zea mays* (NP_001147117.1), *Ginkgo biloba* (AIU48910.1), *Physcomitrella patens* (XP_001783053.1), *Drosophila melanogaster* (NP_611832.1), *Homo sapiens* (NP_060504.1) and *Schizosaccharomyces pombe* (NP_593438.1). The arrow marks the Thr to Ile change. Conserved residues are highlighted in grey; highly conserved residues are highlighted in black.

(c) Seedlings of Col-0, one *ozs3* backcross line and two independent transgenic lines, generated by transforming the BC line with a genomic *OZS3* construct, were grown vertically under control and Zn^{2+} excess (+60 µM) conditions for approximately 7 days. Data represent the mean ± SD of three independent experiments (n = 93–115). Left: absolute root growth. Significant differences from Col-0 were determined by two-way analysis of variance (ANOVA) and Tukey's test (***$P < 0.001$). Right: relative root growth of seedlings as an indicator for tolerance, calculated as root length metal treatment/mean root length control conditions × 100. Significant differences from Col-0 were determined by one-way ANOVA and Tukey's test (***$P < 0.001$). Shown in (d) are seedlings after 7 days cultivation. Scale bar = 1cm.

reporter lines were generated by transforming Col-0 with *GUS* under the control of the *OZS3* promoter (1500 bp). Three independent pOZS3::*GUS* transgenic lines consistently showed staining predominantly of the vasculature in roots and leaves (Figure S7b). According to data queried through the eFP browser (http://bar.utoronto.ca/efp/cgi-bin/efpWeb.cgi), *OZS3* is uniformly expressed in rosette and cauline leaves, roots, stems, flowers and seeds.

OZS3 is an essential gene

To obtain additional *ozs3* alleles, we analyzed T-DNA insertion lines (http://signal.salk.edu/cgi-bin/tdnaexpress). Seedlings of line SALK_065643, carrying an insertion in the *OZS3* promoter, and SALK_038590, carrying an insertion in the 3′-UTR, grew normally on plates and were not investigated further. The same applied to SALK_140479, which, according to our analysis, has an insertion in the *OZS3* promoter, too. Among all the available insertion lines, we could identify only one line (SAIL_241_E09) that carries an insertion within the coding sequence (in exon 1). Surprisingly, however, the plants showed neither Zn^{2+} hypersensitivity, nor any other of the phenotypes observed for *ozs3*. Therefore, we tested the expression of *OZS3* by a quantitative reverse transcriptase-polymerase chain reaction (qRT-PCR) using a primer pair binding downstream of the T-DNA integration site (Figure S8a) and could detect a much higher transcript abundance than in wild-type (Figure S8b). By contrast, using a primer pair binding upstream of the integration site, no signal could be detected, indicating that no full-length mRNA is present in SAIL_241_E09. To explain the absence of *ozs3* phenotypes, we performed rapid amplification of cDNA ends (RACE)-PCR analysis and were able to identify several hybrid mRNAs consisting of a part of the inserted T-DNA and a truncated version of the *OZS3* mRNA. Such hybrid transcripts may give rise to a protein missing the first 42 amino acids of OZS3. To test whether a respective N-terminally truncated protein is functional, we transformed *ozs3* with a corresponding Δ42-OZS3-GFP fusion protein under control of the 35S promoter. Several transgenic lines showed a full complementation of both the Zn^{2+} hypersensitivity and the reduced root growth under control conditions, showing clearly that even the truncated version is functional (Figure S8c). Thus, there are apparently no true knockout alleles of *OZS3* available in the public T-DNA insertion line collections.

A possible explanation for the lack of null alleles could be that the *OZS3* gene is essential. This hypothesis was investigated by employing CRISPR/Cas9 to generate transgenic lines with a frameshift mutation in *OZS3* using two independent target sites (Figure 5a). In the T1 generation, we identified several lines that carried a wild-type and a mutated (1 bp insertion or deletion) allele of *OZS3*. All of the mutations appeared at the predicted position in the first exon (Figure 5b–e). None of the lines heterozygous for a mutated non-functional *OZS3* variant showed full seed set, in contrast to other transgenic lines harboring Cas9 but carrying wild-type *OZS3* (Figure 5f–i). Thus, homozygous loss-of-function mutations in *OZS3* apparently are embryo-lethal. Correspondingly, when we genotyped 20 individuals of the T2 generations, none of these were homozygous for the InDel mutation. All plants were either heterozygous or homozygous wild-type.

OZS3 is a conserved DCAF protein

The protein encoded by *OZS3* belongs to the WD40 superfamily. WD40 domains are characterized by several WD40

© 2020 The Authors.

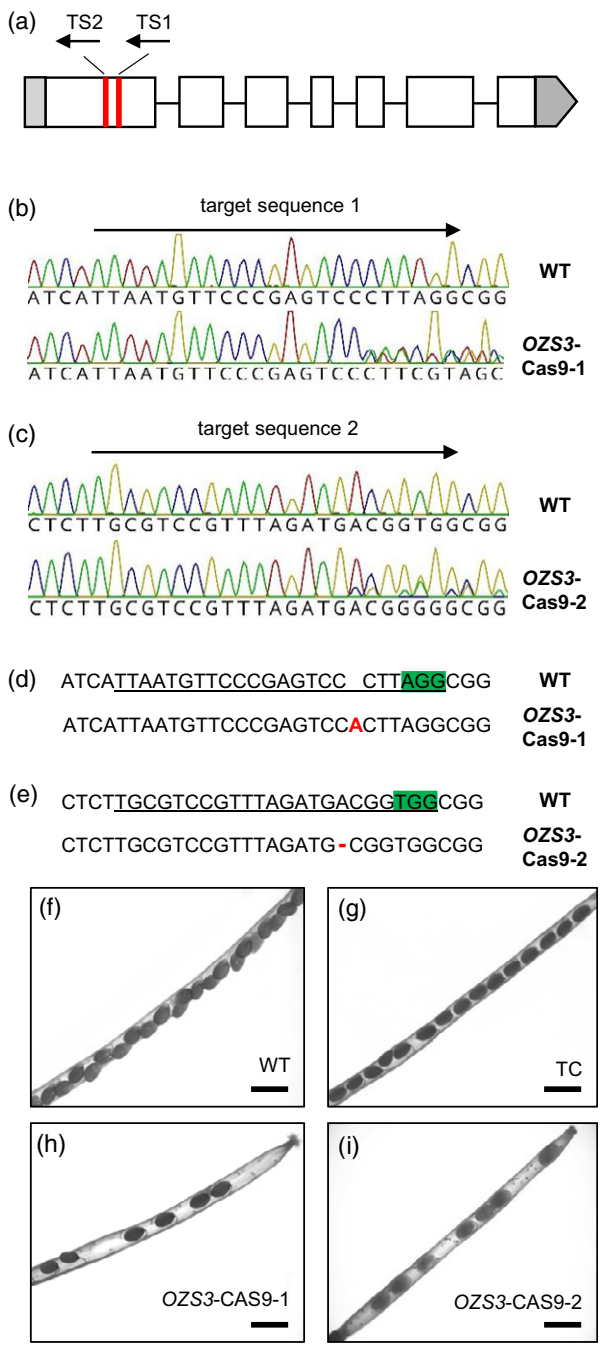

Figure 5. Complete loss of OZS3 function causes embryo lethality. An *OZS3* null allele was generated by CRISPR/Cas9.
(a) Exon intron structure of *OZS3* (white boxes = exons; grey boxes = UTRs); bold red lines mark target sites for Cas9 cleavage.
(b, c) Sequencing files of wild-type and two independent Cas9 lines (T1 generation). Two constructs differing in the target sequence for Cas9 cleavage (target sequences 1 and 2, arrow) were used for transformation. Both target sites are located within the first exon of *OZS3*.
(d, e) Mutations identified in these transgenic plants (T1 generation). The PAM motif is indicated in green. Target sequences are underlined.
(f–i) Siliques of Col-0 (f), a transgenic control (Cas9 line without mutation in *OZS3*) (g) and two independent transgenic lines (h, i), with an insertion or a deletion within the first exon of *OZS3* (*OZS3*-Cas9-1 and *OZS3*-Cas9-2, respectively). Scale bar = 1 mm.

repeats that fold into β-propellers consisting of blades comprising four anti-parallel β-strands. They lack enzymatic activity and are instead often involved in the assembly of functional protein complexes (Stirnimann *et al.*, 2010). OZS3 carries six or seven WD40 domains according to predictions by SMART (http://smart.embl-heidelberg.de) and the WD40 protein database WDSPdb (Wang *et al.*, 2015), respectively. No other characterized protein domains were predicted for OZS3. A search among all *A. thaliana* WD40 proteins placed OZS3 among 85 putative DWD proteins (Lee *et al.*, 2008). The DWD box including the characteristic WDxR motif at the end is found in amino acids 388–403 (Figure 4a). A second incomplete DWD box lacking the terminal arginine (designated DWDΔR) (Lee *et al.*, 2008) is found in amino acids 294–309. According to BLAST searches, no *OZS3* homolog exists in *A. thaliana*, whereas orthologs appear to be present in every higher plant species. This is illustrated when constructing a phylogenetic tree of OZS3-like sequences (Figure 4a; Figure S9). Sequences from a wide range of organisms are more similar to OZS3 than the closest *A. thaliana* sequence At2g19540 (Lee *et al.*, 2008). Also, searches of the HomoloGene (www.ncbi.nlm.nih.gov/homologene) and YOGY (bahlerweb.cs.ucl.ac.uk/YOGY/index.shtml) databases revealed that most eukaryotes with sequenced genomes, for example *Homo sapiens*, *Rattus norvegicus*, *Drosophila melanogaster*, *Caenorhabditis elegans*, *Dictyostelium discoideum*, *Plasmodium falciparum*, *Neurospora crassa* and *Schizosaccharomyces pombe* possess exactly one putative *OZS3* ortholog. Among the few exceptions are *Oryza sativa* and the pufferfish *Takifugu rubripes* with three putative homologs. Many of the predicted proteins are named after *H. sapiens* WDR70 (for WD40 repeat-containing protein 70). None of the putative *OZS3* orthologs in model systems is functionally characterized, with the recent exception of the *S. pombe* ortholog Wdr70 (SPAC343.17c) (Zeng *et al.*, 2016).

OZS3 interacts with DDB1

The presence of a DWD box and the characteristic WDxR motif suggested that OZS3 is a component of a CUL4-E3 ligase complex and serves as a substrate receptor (= DCAF). In testing this hypothesis, we first determined the subcellular localization of OZS3 because it is known, for several DWD proteins, that they are localized in the nucleus (Zhang *et al.*, 2008). We expressed an OZS3-GFP fusion protein under 35S control in *ozs3*. The fusion protein was fully functional (Figure 6a). Using confocal microscopy, a signal consistent with nuclear localization was detected in root cells (Figure 6b–e). The OZS3-GFP fusion protein appeared to be stable because no cytosolic GFP signal was seen. Nuclear localization was independently confirmed through transient expression of CFP-OZS3 fusion proteins in *Nicotiana benthamiana* (Figure 6f–h).

© 2020 The Authors.

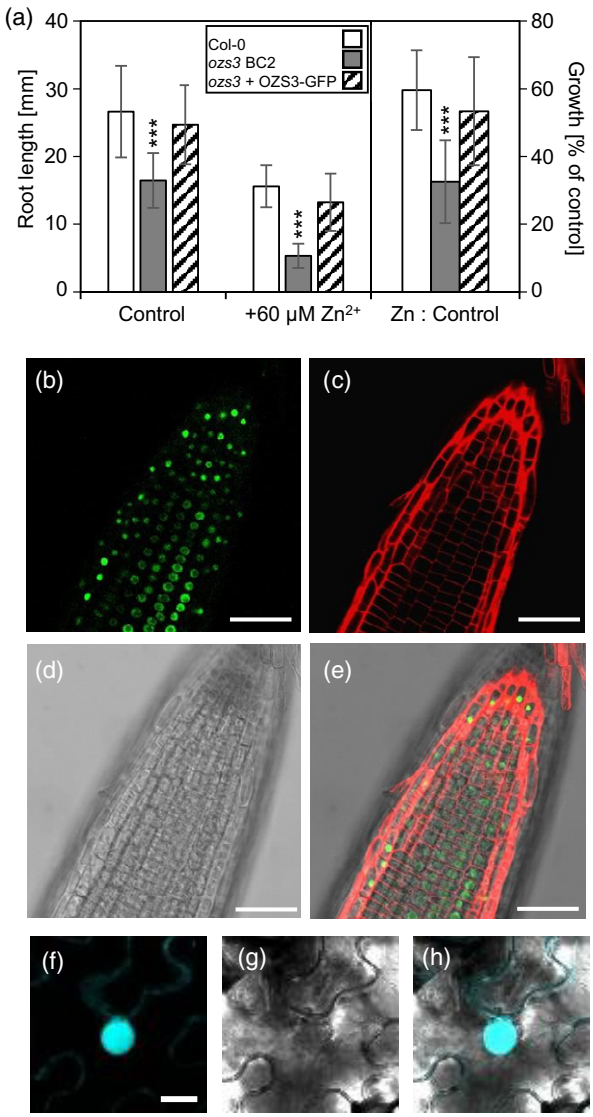

Figure 6. OZS3 is a nuclear protein.
(a) Complementation of *ozs3* Zn^{2+} hypersensitivity by expressing an OZS3-GFP fusion protein under control of the 35S promotor. Seedlings of Col-0, one *ozs3* backcross line (BC) and a respective transgenic line were grown vertically with and without additional 60 µM $ZnSO_4$ for 7 days. Data represent the mean ± SD of three independent experiments (n = 58–73). Left: absolute values. Significant differences from Col-0 were determined by a two-way analysis of variance (ANOVA) and Tukey's test (***$P < 0.001$). Right: relative root growth of seedlings as an indicator for tolerance, calculated as root length metal treatment/mean root length control conditions × 100. Significant differences from Col-0 were determined by one-way ANOVA and Tukey's test (***$P < 0.001$).
(b–e) Representative confocal images of the root tip of the transgenic *ozs3* plant tested for functionality of the OZS3-GFP fusion protein as shown in (a). (b) GFP fluorescence, (c) propidium iodide staining, (d) bright field and (e) overlay. Scale bar = 50 µm. (f–h) Representative confocal images of *Nicotiana benthamiana* leaf epidermal cells transiently expressing a CFP-OZS3 fusion construct under control of the 35S promotor.
(f) CFP-fluorescence, (g) bright field and (h) overlay. Scale bar = 20 µm.

When a version with the amino acid exchange caused by the *ozs3* mutation was expressed, no effect on subcellular localization was found (Figure S10). For DDB1a, localization in the cytosol and the nucleus was observed in accordance with previous studies (Zhang *et al.*, 2008).

As a DCAF protein, OZS3 has to interact with DDB1 *in vivo*. This was investigated first in yeast two-hybrid assays. The results indicated a weak interaction (Figure 7a). Next, we tested interaction by co-expressing OZS3-mVenus and HA-DDB1a in *A. thaliana* protoplasts. Co-immunoprecipitation assays then showed that OZS3-mVenus (calculated molecular weight 98.3 kDa) can effectively precipitate HA-DDB1a (calculated molecular weight 125 kDa), whereas mVenus cannot (Figure 7b). These findings were confirmed after co-infiltrating constructs for GFP-OZS3 and HA-DDB1a into *N. benthamiana* leaves. Again, HA-DDB1a was co-precipitated with GFP-OZS3 (Figure S11). To substantiate the interaction between OZS3 and DDB1a *in planta*, we performed bimolecular fluorescence complementation experiments. A strong YFP signal was detectable in the nucleus of *N. benthamiana* epidermal cells expressing one half of YFP fused to OZS3 and the other half of YFP fused to DDB1a (Figure 7c). As negative controls, we expressed, in accordance with recommendations by Waadt and Kudla (2008), (i) an OZS3 version with a deletion of the entire DWD box and (ii) an OZS3 version with alanine substitutions of amino acids in the WDxR motif essential for interaction of DCAFs with DDB1 (He *et al.*, 2006). To rule out a defect in protein accumulation as a result of mis-folding or a mis-localization of the mutated variants, we checked levels of the recombinant proteins (Figure 7e) and their nuclear localization (Figure S10). No differences to the wild-type protein were detectable. Fluorescence intensity was strongly reduced for OZS3-ΔDWD and OZS3-ADxA, indicating that OZS3 and DDB1a indeed interact *in planta*. Furthermore, interaction of the OZS3 variant corresponding to the protein expressed in the *ozs3* mutant, such as with an amino acid exchange in position 377 from threonine to isoleucine, appeared much weaker than that of the wild-type protein (Figure 7c,d). We concluded from the protein interaction studies that OZS3 is a DCAF, that is, an adaptor protein recruiting substrates to CUL4 E3 ligases via interaction with DDB1.

UV stress sensitivity of the *ozs3* mutant

The only functionally characterized putative *OZS3* ortholog in any biological system is *S. pombe Wdr70*. It has been implicated in DNA damage repair. Loss-of-function mutants are more sensitive to UV and genotoxic treatments (Zeng *et al.*, 2016). We therefore tested the

© 2020 The Authors.

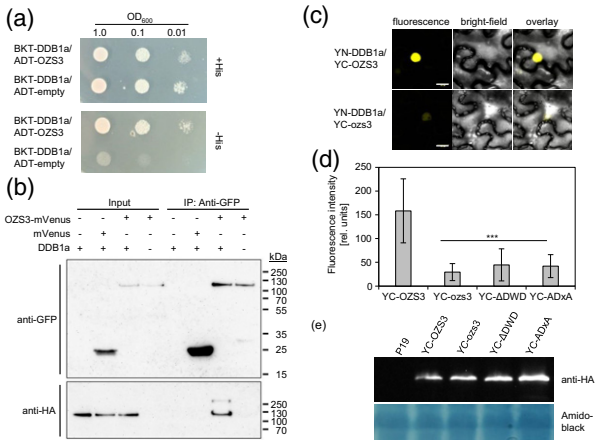

Figure 7. OZS3 interacts with DDB1a *in vivo*.
(a) Yeast two-hybrid assay with BKT-DDB1a (= DDB1a-pGBKT7) and ADT-OZS3 (= OZS3-pGADT7AD). The combination of BKT-DDB1a and ADT-empty served as a negative control. Serial dilutions of yeast cultures (OD_{600} = 1.0, 0.1 and 0.01) were spotted onto YNB medium plus histidine (top) and YNB medium without histidine (bottom).
(b) Co-immunoprecipitation of HA-DDB1a (calculated molecular weight 125 kDa) and OZS3-mVenus (calculated molecular weight 98.3 kDa) transiently co-expressed in *Arabidopsis thaliana* protoplasts. Total protein extracts of protoplasts expressing either OZS3-mVenus alone or OZS3-mVenus and HA-DDB1a were used for co-immunoprecipitation with an anti-GFP antibody. Cells expressing mVenus served as negative controls. The western blot was immunostained using anti-HA (Sigma-Aldrich) and anti-GFP (Roche) antibodies.
(c–e) Bimolecular fluorescence complementation with YN-DDB1a and different variants of YC-OZS3. (c) Confocal image, bright field and overlay of the lower epidermis of *Nicotiana benthamiana* leaves infiltrated with YN-DDB1a and either YC-OZS3 (wild-type sequence) (top) or YC-ozs3 (mutated version) (bottom). Scale bar = 20 μm. (d) Quantification of fluorescence intensity for YN-DDB1a combined with YC-OZS, YC-ozs3, YC-ΔDWD (DWD box deleted) or YC-ADxA (WDxR motif mutated). Data represent the mean ± SD of three independent experiments (n = 56–225). Significant differences from wild-type were determined by one-way analysis of variance and Tukey's test, ***$P < 0.001$. (e) Immunodetection of the OZS3 variants with an anti-HA antibody. Transformation with P19 alone served as negative control; loading control: Amido black staining.

sensitivity of the *ozs3* mutant to UV-C radiation as a form of genotoxic stress. After all exposure times, the survival of *ozs3* seedlings was significantly lower than that of Col-0 (Figure S12), suggesting that OZS3 is also involved in the response to genotoxic stress.

Transcriptome changes in *ozs3*

To obtain leads as to cellular pathways OZS3 may be involved in, we performed root transcriptome comparisons of Col-0 and *ozs3* backcross lines. For the sake of easier access to material, hydroponically grown plants were used. A general growth defect of the *ozs3* mutant was apparent also in 4-week-old plants cultivated hydroponically (Figure S13), allowing for a comparative analysis under control conditions to find constitutively mis-regulated genes in *ozs3*. Furthermore, we investigated the effects of the environmental factor that caused the most dramatic phenotypes in *ozs3*, namely exposure to cold. Plants were exposed to 4°C for 24 h.

The root transcriptomes of Col-0 and *ozs3* plants showed pronounced constitutive differences under control conditions. In total, 183 genes were differentially expressed (69 with higher transcript abundance; 114 with lower transcript abundance in *ozs3*). The only Gene Ontology (GO) terms enriched in this group were 'cellular response to hypoxia', 'response to osmotic stress' and 'oxidation-reduction process'.

Given the metal hypersensitivity of *ozs3*, we specifically looked at annotated metal homeostasis genes (Suryawanshi *et al.*, 2016). Five genes belonging to this group were found to be less active in *ozs3* under control conditions: *OPT3*, *CDF2*, *bHLH39*, *NAS4* and the defensin gene *AFP1*. However, metal homeostasis genes were not significantly enriched among the genes mis-regulated in *ozs3* under control conditions.

Both genotypes responded strongly to the cold treatment (Figure S14). The *ozs3* cold response was inspected by comparing it to the robust cold response for Col-0, which we defined as the overlap between our Col-0 data set and two previously reported transcriptome analyses (Vogel *et al.*, 2005; Kilian *et al.*, 2007). In total, 311 genes were cold-responsive according to all three data sets. Of these, 91% were responsive in *ozs3* as well, suggesting that the *ozs3* growth arrest at 4°C is not caused by a general inability to acclimate to cold.

DISCUSSION

A typical plant genome encodes hundreds of proteins with one or predominantly multiple WD domains. Most of them are widely conserved across the Eukarya, indicating basic cellular functions (van Nocker and Ludwig, 2003). Among the WD domain proteins, a large group consists of putative DCAFs, comprising proteins assumed to be associated with CUL4-DDB1 E3 ligases. One of the putative DCAFs is OZS3. The mutation causing Zn^{2+} hypersensitivity (Figure 1) and the other phenotypes of the isolated *ozs3* line, including compromised growth specifically of the primary root (Figure S4), growth arrest at 4°C (Figure 3), longer petioles (Figure S6) and early flowering (Figure S5), is located in the gene *At2g20330*, one of at least 85 DCAF genes predicted in *A. thaliana* (Lee *et al.*, 2008). This was demonstrated by full complementation of the *ozs3* phenotypes with a construct driving expression of the *OZS3* gene under control of its own promoter (Figure 4; Figure S6).

A typical feature of DCAFs is the presence of several WD domains and the DWD box within one or two of the WD domains. The DWD box mediates interaction with DDB1. A motif within the DWD box is WDxR. Because the conserved aspartate and arginine residues are critical for the docking to DDB1, the WDxR motif is considered a signature sequence of substrate-recruiting WD40 proteins within

© 2020 The Authors.

CUL4 E3 ligase complexes (Angers *et al.*, 2006; He *et al.*, 2006). OZS3 and its orthologs from *O. sativa*, *P. patens*, *H. sapiens* and *D. melanogaster* all possess the WDxR motif (amino acids 400–403 in OZS3). More importantly, OZS3 was shown here to bind to DDB1a *in vivo*. Comparatively weak interaction with DDB1 in yeast two-hybrid assays as found for OZS3 was reported previously for other *A. thaliana* DCAFs. An example is MSI1, a DCAF essential for reproductive development in *A. thaliana* (Dumbliauskas *et al.*, 2011). Independent evidence for interaction was obtained through *in vivo* co-immunoprecipitation experiments in two different experimental systems, namely *A. thaliana* protoplasts (Figure 7b) and *N. benthamiana* leaves (Figure S11). Tagged OZS3 specifically co-precipitated HA-tagged DDB1a. Furthermore, BiFC experiments showed interaction of OZS3 and DDB1a in the nucleus, where OZS3 is localized according to the results obtained with transiently expressed CFP-OZS3 fusions, as well as with the functional OZS3-GFP fusion stably expressed in *ozs3* (Figure 6). Other DCAF proteins have also been detected in the nucleus before (Zhang *et al.*, 2008; Seo *et al.*, 2014). The same applies to the detection of a DDB1 fusion protein in both cytosol and nucleus (Zhang *et al.*, 2008).

The intensity of the fluorescence signal derived from BiFC proteins was strongly reduced when different mutated versions of OZS3 were tested lacking either the complete DWD box or carrying alanines instead of the tryptophan and the arginine in the WDxR motif. Because β-propellers typical for WD40 proteins are prone to mis-folding, we checked that the mutant versions can be detected by immunoblotting (Figure 7e) and are localized to the nucleus (Figure S10). Taken together, OZS3 adds to the limited number of plant DCAF proteins for which interaction with DDB1 has actually been experimentally demonstrated to date. Site-directed mutagenesis confirmed the essential role of the DWD box and especially the WDxR motif for interaction of DCAFs with DDB1 that was shown, for example, in *A. thaliana* and human DCAFs (Rapić-Otrin *et al.*, 2003; Pazhouhandeh *et al.*, 2011). Moreover, the much lower YFP fluorescence detected upon co-expression of the *ozs3* protein version relative to the wild-type OZS3 protein in BiFC experiments, suggested that the mutation in *ozs3* weakens the interaction with DDB1 and thereby compromises function.

In an early classification of *A. thaliana* WD40 domain proteins, OZS3 was placed in its own class with putative orthologs from *H. sapiens* and *D. melanogaster* (van Nocker and Ludwig, 2003). Indeed, *OZS3* orthologs can be found in most eukaryotic genomes, although no homologous sequences are present within the *A. thaliana* genome (Figure S9). The same applies to most other eukaryotic model systems. According to the YOGY database (Penkett *et al.*, 2006) and HomoloGene searches, species from *S. pombe* to *H. sapiens* possess (with very few exceptions) one ortholog. A similar situation was reported for the *A. thaliana* DCAF WDR55 (Bjerkan *et al.*, 2012).

With the exception of the *S. pombe* gene discussed below, no functional data are available for any of the OZS3 orthologs. Loss of the *C. elegans* orthologous gene *gad-1* is embryo-lethal because no gastrulation is initiated (Knight and Wood, 1998). The lack of information on biological functions of WDR70 proteins in animals and plants may indicate that loss-of-function mutants are not viable. The existing evidence supports the notion that *OZS3* is indeed an essential gene and thus the *ozs3* allele isolated in our mutant screen represents a weak allele. Apparently, there is no T-DNA insertion line available for *OZS3* that results in a true knockout. In a large-scale screening of putative *A. thaliana* DCAFs, no phenotype was observed for line SALK_140479 homozygous for an insertion upstream of the *OZS3* coding sequence (Lee *et al.*, 2010). This was confirmed by our analysis for all lines with promoter or UTR insertions. The only line with an exon insertion (SAIL_241_E09) does not appear to represent a null allele. We expressed a protein in *ozs3* that was truncated according to insertion site and transcript sequences found in SAIL_241_E09. This protein fully complemented the growth defect of the *ozs3* mutant (Figure S8), suggesting at least partial functionality of a truncated OZS3 protein in SAIL_241_E09. Similar findings had been reported for the DCAF ABD1. One of the mutant alleles, *abd1-2*, produces a truncated transcript which is suspected to give rise to a partially functional protein (Seo *et al.*, 2014).

The strongest evidence for an essential function of OZS3 comes from the generation of *OZS3* mutants via CRISPR/Cas9. Transgenic plants were generated in Col-0 background. No lines homozygous for a frame shift mutation in *OZS3* were obtained. Abortion of approximately 25% of the seeds was consistent with embryo-lethality.

OZS3 is not transcriptionally responsive to Zn excess (Figure S7). Furthermore, given the essentiality of OZS3, we hypothesize that OZS3 is not part of the Zn homeostasis network *per se*, such that it is not primarily functioning in the distribution of Zn between organs, tissues, cells and cellular compartments. Loss of known Zn homeostasis components such as transporters (e.g. HMA4) (Hussain *et al.*, 2004), enzymes involved in chelator synthesis (e.g. nicotianamine synthase) (Schuler *et al.*, 2012) or transcription factors activating metal responses (e.g. bZIP19/23) (Assuncao *et al.*, 2010) has, to date, not been associated with severe phenotypes or even lethality in the absence of a metal excess or deficiency condition. Even in the presence of such conditions, respective loss-of-function mutants usually survive and only show growth defects and/or ionome changes. This can be explained by the robustness of metal homeostasis networks. Rather than OZS3 being a Zn homeostasis factor, Zn excess aggravates a general growth defect especially of the primary root in

© 2020 The Authors.

ozs3 (Figure 1). This is reminiscent of the *dez1* mutant, which shows de-etiolated hypocotyl growth in the dark when exposed to Zn excess (Sinclair *et al.*, 2017). Consistent with a role outside of Zn homeostasis, the *ozs3* Zn hypersensitivity is not caused by a deregulation of Zn uptake or distribution (Figure S3). Instead, ROS detection and quantification suggested that, in *ozs3* root cells, the oxidative stress triggered by high external Zn^{2+} is less well contained than in wild-type cells. In agreement with previous studies, we did not detect an increase in H_2O_2 concentrations in Zn^{2+} exposed wild-type roots that already showed massively elevated Zn content (Remans *et al.*, 2012). However, *ozs3* roots accumulated significantly more H_2O_2 and O_2^- under these conditions (Figure 2). On the other hand, abiotic stress phenotyping did not produce evidence for a general deficiency of *ozs3* plants to cope with oxidative stress. Indeed, other oxidative stress treatments such as paraquat affected *ozs3* less than the wild-type (Figure S1). Such an apparent gain in relative growth could be a result of reduced growth under control conditions. Currently, we cannot explain the Zn specificity of higher ROS production. It may indicate a loss of control over the cytosolic Zn pool, which would not be detectable when analyzing total Zn levels.

Although high Zn^{2+} concentrations exacerbated the growth defect specifically of the primary root, chilling stress caused a complete growth arrest of *ozs3* mutant plants. Several chilling sensitive (*chs*) *A. thaliana* mutants have been described that are unable to grow when shifted to temperatures lower than between approximately 12 and 18°C (Schneider *et al.*, 1995). Causal genes were often found to represent disease resistance genes of the TIR-NBS class, for example, *chs1* (Wang *et al.*, 2013; Zbierzak *et al.*, 2013), *chs2* (Huang *et al.*, 2010) and *chs3* (Yang *et al.*, 2010). All of these mutants show an over-activation of defense-related cell death pathways during exposure to cold. By contrast to *chs1*, *chs2* and *chs3*, *ozs3* mutants do not die after transfer to low temperatures. Even after 6 weeks of complete growth arrest at 4°C, plants were able to resume growth when shifted back to permissive temperatures (Figure 3), which is similar to the cold-conditional dwarf phenotype reported for a mutant with a defect in REIL1 and REIL2, homologs of a yeast ribosome biogenesis factor (Beine-Golovchuk *et al.*, 2018). Similar to this mutant, *ozs3* showed a wild-type-like transcriptional response to cold (Figure S14). However, unlike for *reil1 reil2*, which activates cold acclimation prematurely at 20°C, we were unable to detect any informative enrichment of GO terms among the genes constitutively mis-regulated in *ozs3*. Thus, following the differentiation between chilling sensitivity caused by a mutation in a cold tolerance gene versus chilling sensitivity as a result of a cold sensitive mutation of an essential gene product (Hugly *et al.*, 1990), we hypothesize that *ozs3* represents an example for the latter category. The mutation apparently renders the encoded protein nonfunctional at low temperature.

Besides a defect in primary root elongation, the *ozs3* mutant shows rather subtle phenotypes at different developmental stages, namely longer petioles and early flowering. This is consistent with a basic cellular function that is perhaps only partially impaired because of the amino acid exchange in OZS3. The diversity and range of *ozs3* phenotypes is reminiscent of another *A. thaliana* DCAF, WDR55. Loss of the *WDR55* gene is lethal because WDR55 function is required for gametogenesis and embryogenesis (Bjerkan *et al.*, 2012). Mutants carrying a weak *wdr55* allele, however, display various less severe phenotypes, such as shorter roots, reduced apical dominance and oddly shaped cotyledons (Bjerkan and Grini, 2013). Furthermore, *WDR55* null mice embryos do not develop beyond day 9.5 (Youngren *et al.*, 2005), a finding that we tentatively predict for respective mammalian WDR70 mutants.

At present, it is only possible to speculate about the exact physiological function of OZS3. No domains other than WD40 can be found in OZS3. Thus, it most probably acts by mediating the interaction between proteins. Plant Cul4-DDB1 E3 ligases and DCAFs have been associated with a wide range of processes, including root development, photomorphogenesis, flowering, circadian rhythm, ABA response, DNA repair and UV response (Choi *et al.*, 2014). Generally, Cul4 E3 ligases can have both proteolytic and non-proteolytic activities. Although DWA1 and 2, as well as ABD1, are hypothesized to act as negative regulators of ABA signaling by triggering the degradation of ABI5 (Lee *et al.*, 2010; Seo *et al.*, 2014), the DCAF MSI1 may be involved in epigenetic processes through non-proteolytic ubiquitylation of unknown targets (Dumbliauskas *et al.*, 2011). A plant DCAF involved in tolerance of a toxic element is ALT2. It is one of several DNA damage response genes required for the growth arrest of roots exposed to aluminum (Chen *et al.*, 2019). ALT2 is hypothesized to be involved in DNA integrity control. DNA damage triggers cell cycle arrest. Loss of ALT2 function can thus partially rescue the growth inhibition of an Al-hypersensitive mutant (Nezames *et al.*, 2012).

Several Cul4 E3 ligases in mammals and a few other species have been implicated in chromatin regulation and genome stability (Jackson and Xiong, 2009). In plants, not only MSI1, but also the DCAF MSI4 have been shown to be involved in gene repression through association with Polycomb-repressing complex2 (Pazhouhandeh *et al.*, 2011). The importance of DDB2 for DNA repair is functionally conserved in Metazoa and plants (Molinier *et al.*, 2008). Recently, the putative *OZS3* ortholog from *S. pombe*, SPAC343.17c, was isolated in a genetic screen for mutants with altered sensitivity to genotoxic agents. *Schizosaccharomyces pombe* Wdr70, as it was named, is recruited to double strand breaks as part of a Cul4-DDB1 complex and

© 2020 The Authors.

stimulates the ubiquitylation of lysine 119 in histone 2 (Zeng *et al.*, 2016). A similar function was proposed for human WDR70. It remains to be determined whether this applies to OZS3 as well. Experimental support that OZS3 may indeed be contributing to DNA integrity was provided by the higher sensitivity of *ozs3* to UV-C exposure, a classic DNA-damaging treatment (Figure S12). The recent observation that chilling stress causes DNA damage predominantly of root stem cells (Hong *et al.*, 2017) possibly connects the cold sensitivity of *ozs3* to DNA damage, too. By contrast, it remains unknown whether Zn excess conditions harm the DNA (Angelé-Martínez *et al.*, 2014).

Identifying potential targets of the putative substrate docking protein OZS3 will be of key importance. However, achieving this has to date been possible for only a small number of DCAFs (Guo *et al.*, 2013; Serrano *et al.*, 2018), especially considering the large number of putative DCAFs in plants and other eukaryotes. For OZS3, it will probably require the isolation or generation of additional alleles, unbiased in-depth analyses of many different plant processes including early root development, and proteomic approaches to directly identify OZS3 targets.

EXPERIMENTAL PROCEDURES

Plant material and cultivation conditions

All of the *A. thaliana* plants used in the present study were in the Col-0 background. The *OZS3* T-DNA insertion lines (SAIL_241_E09, SALK_140479, SALK_065643, SALK_038590 and SALK_132762) were obtained from NASC (http://arabidopsis.info). For transient expression *N. benthamiana* was used.

Arabidopsis thaliana seeds were surface-sterilized and then stratified for 48 h at 4°C in the dark. Plants were cultivated in a modified 1:10 Hoagland medium [0.28 mM $Ca(NO_3)_2$, 0.1 mM $(NH_4)H_2PO_4$, 0.2 mM $MgSO_4$, 0.6 mM KNO_3, 5 μM of a complex of Fe(III) and *N*,*N*′-di-(2-hydroxybenzoyl)-ethylenediamine-*N*,*N*′-diacetate (ABCR GmbH, Karlsruhe, Germany), 5 mM MES, 1% (w/v) sucrose, 1% (w/v) Type-A agar (Sigma-Aldrich, St Louis, MO, USA), pH 5.7]. For root architecture analysis, images were captured after 10–12 days and the length of all primary and secondary roots was determined using IMAGEJ (NIH, Bethesda, MD, USA).

For UV stress treatments, 4–5-day-old seedlings (24 seedlings per Petri dish) were exposed to UV-C light (254 nm, 15 W, at a distance of 80 cm above the seedlings) for 30, 60 or 90 min. After additional cultivation for 5–7 days, survival was scored.

Liquid culture of seedlings was employed to obtain material for the comparison of transcript abundance in different genotypes. Surface-sterilized and stratified seeds were transferred to 50-ml Falcon tubes filled with 10 ml of modified 1:10 Hoagland medium. Seedlings were cultivated at 23°C under long-day conditions (16:8 h light/dark photocycle) and with gentle shaking (60 rpm). After 7–9 days, seedlings were harvested.

For transcriptome comparisons Col-0 wild-type and *ozs3* backcross lines were cultivated in hydroponic culture (modified 1:10 Hoagland medium) under short-day conditions (8:16 h light/dark photocycle) at 23°C in a growth chamber (Percival, Perry, IA, USA). For cold treatment, plants were transferred to 4°C for 24 h prior to root harvest, with control plants remaining at 23 °C.

DNA constructs were transformed into *A. thaliana* Col-0 or the *ozs3* mutant using *Agrobacterium tumefaciens* strain GV3101 and floral dip. For transient expression in *N. benthamiana*, leaves of 5–6 week old plants cultivated on soil under long day conditions (16 h light, 8 h dark) were infiltrated with *A. tumefaciens* suspensions and analyzed after 3 days.

Map-based cloning of *ozs3*, complementation analysis and reporter lines

Genomic DNA isolation and PCR-based mapping were performed using established procedures. Candidate genes from the identified region on chromosome 2 were amplified by PCR and sequenced. For complementation analysis, 1500 bp of the promoter, the coding sequence plus UTRs and 450 bp of the terminator of *At2g20330* were cloned into pMDC123 (Curtis and Grossniklaus, 2003). GFP-fusions with full-length or N-terminally truncated OZS3 were generated by amplifying either the complete coding sequence or a sequence lacking the first 126 nucleotides from cDNA, and cloning into either pMDC83 or pMDC43 (Curtis and Grossniklaus, 2003).

The promotor of *OZS3* (approximately 1.5 kb upstream of ATG) was amplified (for primers, see Table S1) and cloned into pCR8/GW/TOPO (Invitrogen, Carlsbad, CA, USA). For GUS staining, transgenic seedlings were cultivated on agar plates with 1:10 modified Hoagland medium under long day conditions (16:8 h light/dark photocycle, 23°C) for 7–12 days and then stained. For this, seedlings were incubated in 100 mM $NaPO_4$ (pH 7.0) for 1 h. Afterwards, seedlings were transferred to the staining solution [100 mM $NaPO_4$, pH 7.0; 1 mM $K_4[Fe(CN)_6]\times 3H_2O$; 1 mM $K_3[Fe(CN)_6]$; 0.1% (v/v) Triton-X-100; 1 mM X-Gluc] and incubated at 37° for 2–9 h.

ROS detection and quantification

Seedlings grown on agar plates for 15 days were transferred to DAB staining solution [277.7 μM 3,3′-diaminobenzidine; 10 mM Na_2HPO_4, 0.05% (v/v) Tween20, pH 3.0] or NBT staining solution (4.28 mM nitroblue tetrazolium chloride, 10 mM KH_2PO_4, 10 mM NaN_3, pH 7.8) and vacuum infiltrated for 5 min. After vacuum infiltration, seedlings were incubated for additional 4 h in DAB or 2.5 h in NBT staining solution under shaking at room temperature in the dark. Staining solution was replaced by bleaching solution [60% (v/v) ethanol, 20% acetic acid (v/v), 20% glycerol (v/v)] and samples were boiled for 30 min in the dark. Next, bleaching solution was renewed and seedlings were incubated for additional 30 min under shaking at room temperature and in the dark. Afterwards, NBT stained samples were examined under a light microscope. For DAB quantification, seedlings were dried on filter paper and the weight was determined. Samples were than frozen in liquid nitrogen, ground and mixed with 1 ml 0.2 M $HClO_4$. After 5 min of incubation on ice, samples were centrifuged for 10 min at 16 000 ***g*** at 4°C. The absorption of the supernatant was measured photometrically at 450 nm. H_2O_2 concentration was determined using a standard curve (H_2O_2 in DAB staining solution).

Elemental analysis

Roots and shoots of approximately 20-day-old seedlings, grown on plates, were harvested separately. Roots were desorbed using the protocol: 1 × Millipore water, 2 × 20 mM $CaCl_2$, 1 × 10 mM ethylenediaminetetraacetic acid (EDTA), pH 5.7; 1 × Millipore water; each time for 10 min at 4°C. After drying and determination of dry weight, the plant material was digested in 2 ml of 65%

© 2020 The Authors.

HNO_3 and 1 ml of 30% H_2O_2 using a microwave (START 1500; MLS GmbH, Leutkirch im Allgäu, Germany). Element concentrations were measured with an iCAP 6500 (Thermo Fisher Scientific, Waltham, MA, USA).

Subcellular localization

OZS3 and *ozs3* coding sequences without stop codon were PCR amplified using cDNA from roots of Col-0 or *ozs3*, respectively. The *DDB1a* coding sequence without stop codon was PCR amplified using cDNA from roots of Col-0. DNA fragments were cloned into pGEM-T. All cloning PCRs were performed with Phusion DNA-Polymerase (Thermo Fisher Scientific). Then, 5–6-week-old *N. benthamiana* plants were infiltrated with Agrobacteria carrying different CFP-OZS3 fusion constructs.

For experiments with *A. thaliana ozs3* complemented by expression of a functional OZS3-GFP fusion (see above for complementation analysis), seedlings were cultivated using the plate assay set-up. After 7 days of cultivation, seedlings were incubated in a propidium iodide (10 mg l^{-1}) solution to stain the cell wall. GFP, CFP and propidium iodide fluorescence was visualized with a SP5 confocal laser-scanning microscope (Leica Microsystems, Wetzlar, Germany).

Bimolecular fluorescence complementation

DNA fragments of all *OZS3* variants and DDB1a were subcloned into pSPYCE(MR) or pSPYNE173 (Waadt *et al.*, 2008) via *Spe*I and *Xma*I. *Agrobacterium tumefaciens* strains (GV3101) carrying the BiFC constructs were used together with the p19 strain to infiltrate 5–6-week-old *N. benthamiana* plants. Three days after infiltration, epifluorescence in the lower epidermis was analysed using a SP5 confocal laser-scanning microscope (Leica Microsystems). All images were captured with identical instrument settings. Fluorescence intensities (at the position of the nucleus) were quantified using IMAGEJ (NIH).

Co-immunoprecipitation

Mesophyll protoplasts were prepared from 6-week-old *ozs3* rosette plants as described by Wu *et al.* (2009). Per construct combination, 1.8 ml of protoplast suspension containing approximately 5×10^7 cells was transfected with the indicated plasmid combinations at final plasmid concentrations of 16.7 μg ml^{-1} (OZS3-mVenus and mVenus) and 27.8 μg ml^{-1} (3xHA-DDB1a). After overnight expression, cells were pelleted in two aliquots per sample, frozen in liquid nitrogen and resuspended in 300 μl of lysis buffer [50 mM Tris-Cl, pH 7.5; 150 mM NaCl; 5% (v/v) glycerol; 2 mM NaF; 1 mM $Na_4P_2O_7$; 1 mM dithiothreitol (DTT); 1 mM EDTA; 0.05 mM ethylene glycol tetraacetic acid (EGTA); 0.1 % (v/v) Nonidet P-40; 0.05 % sodium deoxycholate; 2 × concentrated Roche cOmplete™ protease inhibitor cocktail; Roche, Basel, Switzerland]. After 30 min of extraction with agitation at 4°C, extracts were diluted with one volume of lysis buffer lacking NaF, $Na_4P_2O_7$, EGTA and detergents, and the cell debris was pelleted twice at 15 000 ***g*** for 10 min. Supernatants derived from corresponding protoplast pellets were combined. Sepharose beads (GE Healthcare, Chicago, IL, USA) coupled with an anti-GFP camel nanobody expressed in *Escherichia coli* and purified via Ni-NTA were equilibrated in wash buffer (adapted from Seo *et al.*, 2014) [50 mM Tris-Cl, pH 7.5; 150 mM NaCl; 5 % glycerol (v/v); 1 mM EDTA; 1 mM DTT] and 15 μl of bead volume was mixed with each sample. The beads were incubated with the extracts under rotation at 4°C for 3 h, and then subsequently washed twice with each 800 μl of wash buffer, and eluted by resuspension in 3× sodium dodecylsulphate (SDS) sample buffer and incubation at 95°C for 5 min. Next, 2.5% of input fractions and 20% (for GFP-detection) or 80% (for HA-detection) of the IP fractions were loaded on SDS-polyacrylamide gels. Western blots were developed using monoclonal anti-GFP antibody (catalog no. 11814460001; Roche) or monoclonal anti-HA antibody (catalog no. H9658; Sigma-Aldrich), in combination with HRP-coupled anti-mouse secondary antibody (catalog no. 4759.1; Carl Roth, Karlsruhe, Germany).

Agrobacterium tumefaciens GV3101 cells carrying OZS3-barII-UT-mTn and 3xHA-DDB1a-pMDC32 were used for transient transformation of 5–6 week old *N. benthamiana* plants. After 3 days, infiltrated leaves were harvested and ground in liquid nitrogen. For extraction of total soluble protein 1.5 ml of extraction puffer (25 mM Tris-HCl, pH 7.5, 150 mM NaCl, 5% (v/v) glycerol, 0.05% (v/v) octylphenoxypolyethoxyethanol, 2.5 mM EDTA, 1× protease inhibitor) was added to 0.5 g of plant material. The suspension was centrifuged for 20 min (16 000 ***g***, 4°C). Supernatant was incubated with GFP-Trap®_MA (Chromotek, Munich, Germany). Protein pull-down was carried out in accordance with the manufacturer's instructions. Washing steps after protein binding were omitted. For elution, precipitates were resuspended in 2 × SDS loading buffer [100 mM Tris-HCl, pH 6.8, 100 mM DTT, 20% (v/v) glycerol, 0.2% bromophenol blue, 2% (w/v) SDS] and boiled for 10 min. Then, 8 μl of total soluble protein (= input) and 20 μl of eluted precipitates were loaded. For immunostaining, primary anti-GFP antibody (11 814 460 001; Roche) was diluted 1:1000, anti-HA (H9658; Sigma-Aldrich) was diluted 1:3000 and secondary antibody (anti-mouse, A9044; Sigma-Aldrich) coupled to peroxidase was diluted 1:10 000. Signals were detected using an enhanced chemiluminescence kit (GE Healthcare).

Yeast two-hybrid assays

Full-length coding sequences of OZS3 and DDB1a were subcloned into pGADT7AD or pGBKT7 (Clontech, Mountain View, CA, USA), respectively. Yeast two-hybrid assays were performed in accordance with the manufacturer's instructions. pGAT7 AD/pGBKT7 combinations were co-transformed into Y2H-Gold cells (Clontech). Transformants were selected by growth on YNB -leu -trp plates. For drop assays, different dilutions were spotted on YNB -leu -trp plates with (control) or without histidine.

RNA extraction, qRT-PCR and RACE-PCR

RNA was extracted with Trizol (Invitrogen) in accordance with the manufacturer's instructions. RNA quality was checked with a NanoPhotometer (IMPLEN, Munich, Germany). DNaseI treated RNA (0.5 μg) was used for cDNA synthesis (PrimeScript™ RT Master Mix; Clontech). qRT-PCR reactions were performed in 96-well plates in a Bio-Rad iCycler with a MyiQ real-time PCR detection system using SYBR Green (iQ SYBR Green supermix; Bio-Rad, Munich, Germany) as described previously (Deinlein *et al.*, 2012). Primers (Table S1) were designed using PRIMER3 (http://primer3.sourceforge.net). 5′-RACE was carried out in accordance with the manufacturer's instructions (SMART™ RACE cDNA amplification Kit; Clontech).

Microarray protocol

Hybridization data from three independent biological replicates were generated for each plant line and condition. Total RNA was extracted using the RNeasy Plant Mini Kit (Qiagen, Valencia, CA, USA). Microarray analyses with an Affymetrix ATH1 chip (Thermo Fisher Scientific) were performed as described previously (Deinlein *et al.*, 2012). As confidence threshold, an adjusted A value of $P < 0.05$ was used and a gene was considered as up- or

© 2020 The Authors.

downregulated when a $\geq$ 2-fold change was given. Microarray data were deposited in the Gene Expression Omnibus database (http://www.ncbi.nlm.nih.gov/geo) under accession GSE113547.

For the identification of overrepresented GO terms, the 'Panther Classification system' was used (Mi *et al.*, 2019). GO terms were classified as significantly overrepresented when adjusted $P < 0.05$.

Generation of an *ozs3* knockout by CRISPR/Cas9

For the identification of CRISPR/Cas9 target sites in *OZS3*, the CCTop online tool (Stemmer *et al.*, 2015) was used. Two sequences in the first exon were chosen that do not overlap and for which no off target sites were predicted (Target sequence 1: TTAATGTTCCCGAGTCCCTTAGG; target sequence 2: TGCGTCCGTTTAGATGACGGTGG). For each target sequence, primer pairs were designed that form a dimer with two *Bsa*I overhangs (Table S1). These dimers were ligated separately into pKSE401 (Xing *et al.*, 2014). Col-0 plants were transformed with the two independent constructs differing in target sequence. To check for mutations in *OZS3*, genomic DNA was extracted from leaves and a fragment was PCR amplified that included both Cas9 target sites. These PCR products were sequenced to detect frameshift mutations in *OZS3*. PCR products indicating a frameshift were cloned into pGEM-T (Promega, Madison, WI, USA) and several resulting plasmids were sequenced to identify the different *OZS3* variants.

ACKNOWLEDGEMENTS

This work was financially supported by the University of Bayreuth. We thank Christiane Meinen and Pia Schuster for their excellent technical assistance, as well as Angelika Mustroph for help with the microarray data analysis. S.C. is grateful to the Schroeder lab at UC San Diego, and especially former lab members Rainer Waadt, Henning Kunz and Benjamin Brandt for advice and fruitful discussions.

CONFLICT OF INTERESTS

The authors declare that they have no competing interests.

AUTHOR CONTRIBUTIONS

MW, BB and NN characterized the *ozs3* mutant, assisted by SS; BB mapped and cloned the *ozs3* gene; NN and MK performed protein–protein interactions studies with assistance from JH and generated deletion mutants using CRISPR-Cas9; SC conceived the project, planned all of the experiments, supervised them together with MW, and wrote the article with contributions from all of the authors.

DATA AVAILABILITY STATEMENT

Microarray data have been deposited in the Gene Expression Omnibus database (http://www.ncbi.nlm.nih.gov/geo/) under accession GSE113547. All other relevant data can be found within the manuscript and its supporting materials.

SUPPORTING INFORMATION

Additional Supporting Information may be found in the online version of this article.

Figure S1. The *ozs3* mutant shows metal hypersensitivity specifically toward Zn^{2+} and is not more sensitive than wild-type to osmotic, salt and oxidative stress.

Figure S2. Dose-dependence of *ozs3* Zn^{2+} hypersensitivity.

Figure S3. Zn accumulation and distribution are not altered in *ozs3*.

Figure S4. *ozs3* seedlings show altered root morphology.

Figure S5. *ozs3* plants flower early.

Figure S6. Complementation of *ozs3* phenotypes by a genomic *OZS3* construct.

Figure S7. *OZS3* expression analysis.

Figure S8. SAIL_241_E09 is a pseudo knockout line.

Figure S9. Phylogenetic tree of OZS3-like sequences.

Figure S10. Subcellular localization of OZS3 variants and DDB1a.

Figure S11. Independent confirmation of co-immunoprecipitation results for OZS3 and DDB1a.

Figure S12. The *ozs3* mutant is UV hypersensitive.

Figure S13. Growth defect of hydroponically grown *ozs3* mutant plants.

Figure S14. The cold responses of Col-0 and *ozs3* showed substantial overlaps.

Table S1. Primer sequences.

REFERENCES

Alloway, B.J. (2008) *Zinc in Soils and Crop Nutrition*, 2nd ed. Brussels/Paris: IZA and IFA.

Andreini, C., Banci, L., Bertini, I. and Rosato, A. (2006) Zinc through the three domains of life. *J. Proteome Res.* **5**, 3173–3178.

Angelé-Martínez, C., Goodman, C. and Brumaghim, J. (2014) Metal-mediated DNA damage and cell death: mechanisms, detection methods, and cellular consequences. *Metallomics*, **6**, 1358–1381.

Angers, S., Li, T., Yi, X.H., Maccoss, M.J., Moon, R.T. and Zheng, N. (2006) Molecular architecture and assembly of the DDB1-CUL4a ubiquitin ligase machinery. *Nature*, **443**, 590–593.

Arrivault, S., Senger, T. and Krämer, U. (2006) The Arabidopsis metal tolerance protein AtMTP3 maintains metal homeostasis by mediating Zn exclusion from the shoot under Fe deficiency and Zn oversupply. *Plant J.* **46**, 861–879.

Assuncao, A.G.L., Herrero, E., Lin, Y.F. *et al.* (2010) Arabidopsis thaliana transcription factors bzip19 and bzip23 regulate the adaptation to zinc deficiency. *Proc. Natl Acad. Sci. USA*, **107**, 10296–10301.

Beine-Golovchuk, O., Firmino, A.A.P., Dąbrowska, A., Schmidt, S., Erban, A., Walther, D., Zuther, E., Hincha, D.K. and Kopka, J. (2018) Plant temperature acclimation and growth rely on cytosolic ribosome biogenesis factor homologs. *Plant Physiol.* **176**, 2251–2276.

Bernhardt, A., Mooney, S. and Hellmann, H. (2010) Arabidopsis DDB1a and DDB1b are critical for embryo development. *Planta*, **232**, 555–566.

Biedermann, S. and Hellmann, H. (2011) WD40 and CUL4-based E3 ligases: lubricating all aspects of life. *Trends Plant Sci.* **16**, 38–46.

Bjerkan, K.N. and Grini, P.E. (2013) The Arabidopsis DDB1 interacting protein WDR55 is required for vegetative development. *Plant Signal. Behav.* **8**, e25347.

Bjerkan, K.N., Jung-Roméo, S., Jürgens, G., Genschik, P. and Grini, P.E. (2012) Arabidopsis WD REPEAT DOMAIN55 interacts with DNA DAMAGED BINDING PROTEIN1 and is required for apical patterning in the embryo. *Plant Cell*, **24**, 1013–1033.

Chen, P., Sjogren, C.A., Larsen, P.B. and Schnittger, A. (2019) A multi-level response to DNA damage induced by aluminium. *Plant J.* **98**, 479–491.

Choi, C.M., Gray, W.M., Mooney, S. and Hellmann, H. (2014) Composition, roles, and regulation of cullin-based ubiquitin e3 ligases. *Arabidopsis Book*, **12**, e0175.

Clemens, S. (2006) Toxic metal accumulation, responses to exposure and mechanisms of tolerance in plants. *Biochimie*, **88**, 1707–1719.

© 2020 The Authors.

Curtis, M.D. and Grossniklaus, U. (2003) A gateway cloning vector set for high-throughput functional analysis of genes in planta. *Plant Physiol.* **133**, 462–469.

Deinlein, U., Weber, M., Schmidt, H. *et al.* (2012) Elevated nicotianamine levels in Arabidopsis halleri roots play a key role in zinc hyperaccumulation. *Plant Cell*, **24**, 708–723.

Deshaies, R.J. and Joazeiro, C.A.P. (2009) RING domain E3 ubiquitin ligases. *Annu. Rev. Biochem.* **78**, 399–434.

Dumbliauskas, E., Lechner, E., Jaciubek, M. *et al.* (2011) The Arabidopsis CUL4-DDB1 complex interacts with MSI1 and is required to maintain MEDEA parental imprinting. *EMBO J.* **30**, 731–743.

Guo, L., Nezames, C.D., Sheng, L., Deng, X. and Wei, N. (2013) Cullin-RING Ubiquitin ligase family in plant abiotic stress pathways. *J. Integr. Plant Biol.* **55**, 21–30.

Haydon, M.J. and Cobbett, C.S. (2007) A novel major facilitator superfamily protein at the tonoplast influences zinc tolerance and accumulation in Arabidopsis. *Plant Physiol.* **143**, 1705–1719.

He, Y.Z.J., Mccall, C.M., Hu, J., Zeng, Y.X. and Xiong, Y. (2006) DDB1 functions as a linker to recruit receptor WD40 proteins to CUL4-ROC1 ubiquitin ligases. *Genes Dev.* **20**, 2949–2954.

Hong, J.H., Savina, M., Du, J., Devendran, A., Kannivadi Ramakanth, K., Tian, X., Sim, W.S., Mironova, V.V. and Xu, J. (2017) A sacrifice-for-survival mechanism protects root stem cell niche from chilling stress. *Cell*, **170**, 102–113.

Hua, Z. and Vierstra, R.D. (2011) The Cullin-RING Ubiquitin-Protein Ligases. *Annu. Rev. Plant Biol.* **62**, 299–334.

Huang, X., Li, J., Bao, F., Zhang, X. and Yang, S. (2010) A gain-of-function mutation in the Arabidopsis disease resistance gene RPP4 confers sensitivity to low temperature. *Plant Physiol.* **154**, 796–809.

Hugly, S., McCourt, P., Browse, J., Patterson, G.W. and Somerville, C. (1990) A chilling sensitive mutant of Arabidopsis with altered steryl-ester metabolism. *Plant Physiol.* **93**, 1053–1062.

Hussain, D., Haydon, M.J., Wang, Y., Wong, E., Sherson, S.M., Young, J., Camakaris, J., Harper, J.F. and Cobbett, C.S. (2004) P-type ATPase heavy metal transporters with roles in essential zinc homeostasis in Arabidopsis. *Plant Cell*, **16**, 1327–1339.

Jackson, S. and Xiong, Y. (2009) CRL4s: the CUL4-RING E3 ubiquitin ligases. *Trends Biochem. Sci.* **34**, 562–570.

Kambe, T., Tsuji, T., Hashimoto, A. and Itsumura, N. (2015) The physiological, biochemical, and molecular roles of zinc transporters in zinc homeostasis and metabolism. *Physiol. Rev.* **95**, 749–784.

Kawachi, M., Kobae, Y., Mori, H., Tomioka, R., Lee, Y. and Maeshima, M. (2009) A mutant strain Arabidopsis thaliana that lacks vacuolar membrane zinc transporter MTP1 revealed the latent tolerance to excessive zinc. *Plant Cell Physiol.* **50**, 1156–1170.

Kilian, J., Whitehead, D., Horak, J. *et al.* (2007) The AtGenExpress global stress expression data set: protocols, evaluation and model data analysis of UV-B light, drought and cold stress responses. *Plant J.* **50**, 347–363.

Knight, J.K. and Wood, W.B. (1998) Gastrulation initiation in Caenorhabditis elegans requires the function of gad-1, which encodes a protein with WD repeats. *Develop. Biol.* **198**, 253–265.

Kopittke, P.M., Blamey, F.P.C., Asher, C.J. and Menzies, N.W. (2010) Trace metal phytotoxicity in solution culture: a review. *J. Exp. Bot.* **61**, 945–954.

Krężel, A. and Maret, W. (2016) The biological inorganic chemistry of zinc ions. *Arch. Biochem. Biophys.* **611**, 3–19.

Kühnlenz, T., Hofmann, C., Uraguchi, S., Schmidt, H., Schempp, S., Weber, M., Lahner, B., Salt, D.E. and Clemens, S. (2016) Phytochelatin synthesis promotes leaf Zn accumulation of Arabidopsis thaliana plants grown in soil with adequate Zn supply and is essential for survival on Zn-contaminated soil. *Plant Cell Physiol.* **57**, 2342–2352.

Lanquar, V., Grossmann, G., Vinkenborg, J.L., Merkx, M., Thomine, S. and Frommer, W.B. (2014) Dynamic imaging of cytosolic zinc in Arabidopsis roots combining FRET sensors and RootChip technology. *New Phytol.* **202**, 198–208.

Lee, J. and Zhou, P.B. (2007) DCAFs, the missing link of the CUL4-DDB1 ubiquitin ligase. *Mol. Cell*, **26**, 775–780.

Lee, J.H., Terzaghi, W., Gusmaroli, G., Charron, J.B.F., Yoon, H.J., Chen, H.D., He, Y.J., Xiong, Y. and Deng, X.W. (2008) Characterization of Arabidopsis and rice DWD proteins and their roles as substrate receptors for CUL4-RING E3 ubiquitin ligases. *Plant Cell*, **20**, 152–167.

Lee, J.H., Yoon, H.J., Terzaghi, W., Martinez, C., Dai, M.Q., Li, J.G., Byun, M.O. and Deng, X.W. (2010) DWA1 and DWA2, two Arabidopsis DWD protein components of CUL4-based E3 ligases, act together as negative regulators in ABA signal transduction. *Plant Cell*, **22**, 1716–1732.

Maret, W. (2017) Zinc in cellular regulation: the nature and significance of "zinc signals". *Int. J. Mol. Sci.* **18**, 2285.

Mi, H., Muruganujan, A., Huang, X., Ebert, D., Mills, C., Guo, X. and Thomas, P.D. (2019) Protocol Update for large-scale genome and gene function analysis with the PANTHER classification system (v.14.0). *Nat. Protoc.* **14**, 703–721.

Molinier, J., Lechner, E., Dumbliauskas, E. and Genschik, P. (2008) Regulation and role of Arabidopsis CUL4-DDB1A-DDB2 in maintaining genome integrity upon UV stress. *PLoS Genet.* **4**, e1000093.

Nagajyoti, P.C., Lee, K.D. and Sreekanth, T.V.M. (2010) Heavy metals, occurrence and toxicity for plants: a review. *Environ. Chem. Lett.* **8**, 199–216.

Nezames, C.D., Sjogren, C.A., Barajas, J.F. and Larsen, P.B. (2012) The Arabidopsis cell cycle checkpoint regulators TANMEI/ALT2 and ATR mediate the active process of aluminum-dependent root growth inhibition. *Plant Cell*, **24**, 608–621.

van Nocker, S. and Ludwig, P. (2003) The WD-repeat protein superfamily in Arabidopsis: conservation and divergence in structure and function. *BMC Genom.* **4**, 50.

Pazhouhandeh, M., Molinier, J., Berr, A. and Genschik, P. (2011) MSI4/FVE interacts with CUL4G-DDB1 and a PRC2-like complex to control epigenetic regulation of flowering time in Arabidopsis. *Proc. Natl. Acad. Sci. USA*, **108**, 3430–3435.

Penkett, C.J., Morris, J.A., Wood, V. and Bähler, J. (2006) YOGY: a web-based, integrated database to retrieve protein orthologs and associated Gene Ontology terms. *Nucleic Acids Res.* **34**, W330–W334.

Rapić-Otrin, V., Navazza, V., Nardo, T., Botta, E., McLenigan, M., Bisi, D.C., Levine, A.S. and Stefanini, M. (2003) True XP group E patients have a defective UV-damaged DNA binding protein complex and mutations in DDB2 which reveal the functional domains of its p48 product. *Hum. Mol. Genet.* **12**, 1507–1522.

Remans, T., Opdenakker, K., Guisez, Y., Carleer, R., Schat, H., Vangronsveld, J. and Cuypers, A. (2012) Exposure of Arabidopsis thaliana to excess Zn reveals a Zn-specific oxidative stress signature. *Environ. Exp. Bot.* **84**, 61–71.

Ren, H., Han, J., Yang, P. *et al.* (2019) Two E3 ligases antagonistically regulate the UV-B response in Arabidopsis. *Proc. Natl. Acad. Sci. USA*, **116**, 4722–4731.

Schneider, J., Hugly, S. and Somerville, C. (1995) Chilling-sensitive mutants of Arabidopsis. *Plant Mol. Biol. Rep.* **13**, 11–17.

Schroeder, D.F., Gahrtz, M., Maxwell, B.B., Cook, R.K., Kan, J.M., Alonso, J.M., Ecker, J.R. and Chory, J. (2002) De-etiolated 1 and damaged DNA binding protein 1 interact to regulate Arabidopsis photomorphogenesis. *Curr. Biol.* **12**, 1462–1472.

Schuler, M., Rellán-Álvarez, R., Fink-Straube, C., Abadía, J. and Bauer, P. (2012) Nicotianamine functions in the phloem-based transport of iron to sink organs, in pollen development and pollen tube growth in Arabidopsis. *Plant Cell*, **24**, 2380–2400.

Seo, K.-I., Lee, J.-H., Nezames, C.D., Zhong, S., Song, E., Byun, M.-O. and Deng, X.W. (2014) ABD1 is an Arabidopsis DCAF substrate receptor for CUL4-DDB1–based E3 ligases that acts as a negative regulator of abscisic acid signaling. *Plant Cell*, **26**, 695–711.

Serrano, I., Campos, L. and Rivas, S. (2018) Roles of E3 ubiquitin-ligases in nuclear protein homeostasis during plant stress responses. *Front. Plant Sci.* **9**, 139.

Shu, K. and Yang, W. (2017) E3 ubiquitin ligases: Ubiquitous actors in plant development and abiotic stress responses. *Plant Cell Physiol.* **58**, 1461–1476.

Sinclair, S.A. and Krämer, U. (2012) The zinc homeostasis network of land plants. *Biochim. Biophys. Acta*, **1823**, 1553–1567.

Sinclair, S.A., Larue, C., Bonk, L. *et al.* (2017) Etiolated seedling development requires repression of photomorphogenesis by a small cell-wall-derived dark signal. *Curr. Biol.* **27**, 3403–3418.

© 2020 The Authors.

Stemmer, M., Thumberger, T., Del Sol Keyer, M., Wittbrodt, J. and Mateo, J.L. (2015) CCTop: an intuitive, flexible and reliable CRISPR/Cas9 target prediction tool. *PLoS ONE*, **10**, e0124633.

Stirnimann, C.U., Petsalaki, E., Russell, R.B. and Müller, C.W. (2010) WD40 proteins propel cellular networks. *Trends Biochem. Sci.* **35**, 565–574.

Suryawanshi, V., Talke, I.N., Weber, M., Eils, R., Brors, B., Clemens, S. and Krämer, U. (2016) Between-species differences in gene copy number are enriched among functions critical for adaptive evolution in Arabidopsis halleri. *BMC Genom.* **17**, 3319.

Vogel, J.T., Zarka, D.G., Van Buskirk, H.A., Fowler, S.G. and Thomashow, M.F. (2005) Roles of the CBF2 and ZAT12 transcription factors in configuring the low temperature transcriptome of Arabidopsis. *Plant J.* **41**, 195–211.

Waadt, R. and Kudla, J. (2008) In planta visualization of protein interactions using bimolecular fluorescence complementation (BiFC). *Cold Spring Harbor Protoc.* **2008**(5), pdb.prot4995. https://doi.org/10.1101/pdb.prot4995

Waadt, R., Schmidt, L.K., Lohse, M., Hashimoto, K., Bock, R. and Kudla, J. (2008) Multicolor bimolecular fluorescence complementation reveals simultaneous formation of alternative CBL/CIPK complexes in planta. *Plant J.* **56**, 505–516.

Wang, Y., Hu, X.-J., Zou, X.-D., Wu, X.-H., Ye, Z.-Q. and Wu, Y.-D. (2015) WDSPdb: a database for WD40-repeat proteins. *Nucleic Acids Res.* **43**, D339–D344.

Wang, Y., Zhang, Y., Wang, Z., Zhang, X. and Yang, S. (2013) A missense mutation in CHS1, a TIR-NB protein, induces chilling sensitivity in Arabidopsis. *Plant J.* **75**, 553–565.

Weber, M., Deinlein, U., Fischer, S., Rogowski, M., Geimer, S., Tenhaken, R. and Clemens, S. (2013) A mutation in the Arabidopsis thaliana cell wall biosynthesis gene pectin methylesterase 3 as well as its aberrant expression cause hypersensitivity specifically to Zn. *Plant J.* **76**, 151–164.

Wu, F.H., Shen, S.C., Lee, L.Y., Lee, S.H., Chan, M.T. and Lin, C.S. (2009) Tape-Arabidopsis Sandwich - a simpler Arabidopsis protoplast isolation method. *Plant Methods*, **5**, 16. https://doi.org/10.1186/1746-4811-5-16.

Xing, H.-L., Dong, L., Wang, Z.-P., Zhang, H.-Y., Han, C.-Y., Liu, B., Wang, X.-C. and Chen, Q.-J. (2014) A CRISPR/Cas9 toolkit for multiplex genome editing in plants. *BMC Plant Biol.* **14**, 327.

Yang, H., Shi, Y., Liu, J., Guo, L., Zhang, X. and Yang, S. (2010) A mutant CHS3 protein with TIR-NB-LRR-LIM domains modulates growth, cell death and freezing tolerance in a temperature-dependent manner in Arabidopsis. *Plant J.* **63**, 283–296.

Youngren, K.K., Coveney, D. and Peng, X. *et al.* (2005) The Ter mutation in the dead end gene causes germ cell loss and testicular germ cell tumours. *Nature*, **435**, 360–364.

Zbierzak, A.M., Porfirova, S., Griebel, T., Melzer, M., Parker, J.E. and Dörmann, P. (2013) A TIR–NBS protein encoded by Arabidopsis Chilling Sensitive 1 (CHS1) limits chloroplast damage and cell death at low temperature. *Plant J.* **75**, 539–552.

Zeng, M., Ren, L., Mizuno, K. *et al.* (2016) CRL4(Wdr70) regulates H2B monoubiquitination and facilitates Exo1-dependent resection. *Nature Commun.* **7**, 11364.

Zhang, Y., Feng, S.H., Chen, F.F., Chen, H.D., Wang, J., Mccall, C., Xiong, Y. and Deng, X.W. (2008) Arabidopsis DDB1-CUL4 associated factor1 forms a nuclear E3 ubiquitin ligase with DDB1 and CUL4 that is involved in multiple plant developmental processes. *Plant Cell*, **20**, 1437–1455.

Zhao, F.-J., Ma, Y., Zhu, Y.-G., Tang, Z. and McGrath, S.P. (2015a) Soil contamination in China: current status and mitigation strategies. *Environ. Sci. Technol.* **49**, 750–759.

Zhao, L., Oliver, E., Maratou, K. *et al.* (2015b) The zinc transporter ZIP12 regulates the pulmonary vascular response to chronic hypoxia. *Nature*, **524**, 356–360.

Zlobin, I.E., Kartashov, A.V., Nosov, A.V., Fomenkov, A.A. and Kuznetsov, V.V. (2019) The labile zinc pool in plant cells. *Funct. Plant Biol.* **46**(9), 796. https://doi.org/10.1071/FP19064

© 2020 The Authors.